International Journal on Science and Technology (IJSAT)
E-ISSN: 2229-7677 ● Website: www.ijsat.org ● Email: editor@ijsat.org

Photo-luminescence study of Dy^{3+} activated $Sr_5(PO_4)_3F$ phosphor synthesized by combustion method

Shashi Sahu[1], Anil Kumar Choubey[2], Abhishek Kumar Mishra[3]

[1]Research scholar, Department of Physics, Govt. V.Y.T. P.G. Autonomous College, Durg , India
[2]Assistant professor, Department of Physics, M.J. College, Bhilai, Durg, India
[3]Assistant professor, Department of Physics, Govt. V.Y.T. P.G. Autonomous College, Durg, India

Abstract
In this study the rare earth Dy^{3+} activated $Sr_5(PO_4)_3F$ phosphor synthesized by combustion method. This phosphor were characterized by XRD, FTIR, SEM, PL and TL for structural, functional-group, morphological and luminescent properties. This phosphor shows its characteristics of X-ray diffraction hexagonal structure with space group $P6_3/m$ and observed crystallite size of 15.3nm match with JCPDS card no. 17-0609. The FTIR spectrum (absorbance) of the synthesized $Sr_5(PO_4)_3F$: Dy^{3+} phosphor exhibits a well-resolved triplet at 435, 441, and 457 cm^{-1}. These peaks are successfully assigned to the bending movements of the phosphate tetrahedral (PO_4^{3-}) groups. The observed crystal splitting into three separate peaks happens because the crystal shape is slightly changed or distorted. Furthermore, the sharpness of these bands strongly verifies the formation of a highly crystalline host lattice. SEM revealed irregular, porous particles in the micrometer range. The optical study of PL, the PL emission at 575 nm due to $^4F_{9/2} \rightarrow {}^6H_{13/2}$ transitions, respectively and PL excitation at 350 and 365 nm observed. This Dy^{3+} activated SFAP fluorapatite phosphor is provides an excellent environment for capturing light from standard commercial near-UV - LED chips, signaling its utility in solid-state lighting applications.

Keywords: combustion method, functional group, Photo-luminescence, solid-state lighting.

1. Introduction

The development of next-generation solid-state lighting, particularly white light-emitting diodes (w-LEDs), has sparked widespread research into high-efficiency luminescent materials. Traditional w-LED architectures often rely on combining a blue LED chip with a yellow-emitting phosphor, which frequently suffers from a low color rendering index (CRI) and poor thermal stability over prolonged operation. To overcome these operational drawbacks, current efforts are shifting toward near-ultraviolet (near-UV) LED chips coupled with multi-color emitting phosphors, a configuration that delivers much better color uniformity and superior spectral control. [1-3].

Among the various host matrices evaluated for these setups, alkaline earth fluorophosphates—specifically Strontium Fluorophosphate, $Sr_5(PO_4)_3F$—have emerged as exceptional candidates. This material crystallizes into a highly stable hexagonal apatite structure, offering excellent thermal endurance, exceptional chemical durability, and a wide bandgap. Its rigid crystal framework provides

distinct coordination environments where host Sr^{2+} ions can be readily substituted by rare-earth activators without destabilizing the overarching lattice structure.

Among the rare-earth ions, trivalent Dysprosium (Dy^{3+}) is uniquely suited for designing single-composition phosphors. The electronic configuration of Dy^{3+} typically gives rise to two primary emission bands in the visible spectrum: a blue emission corresponding to the $^4F_{9/2} \rightarrow {}^6H_{15/2}$ magnetic dipole transition, and a highly intense yellow emission originating from the $^4F_{9/2} \rightarrow {}^6H_{13/2}$ hypersensitive electric dipole transition. By carefully adjusting the local coordination and host environment, the intensity ratio of these blue and yellow emissions can be tuned to achieve near-ideal white light emission.[4-7].

This study explores the synthesis, microstructural characteristics, and luminescent behaviors of a nanostructured $Sr_5(PO_4)_3F:Dy^{3+}$ phosphor system. By investigating the structural framework through SEM and XRD, along with systematic concentration optimization via photoluminescence (PL) spectroscopy, this work establishes a clear correlation between nanoscale morphology and optical performance for advanced display and solid-state lighting applications.[10].

2. Experimental

The Dy^{3+} activated $Sr_5(PO_4)_3F$ phosphors have been prepared by combustion synthesis. The starting AR grade materials (99.99% purity) are calcium nitrate tetrahydrated (Sr(NO3)2).4H_2O, ammonium di-hydrogen phosphate ($NH_4H_2PO_4$), ammonium fluoride (NH_4F), dysprosium (Dy_2O_3), and urea (NH_2CONH_2) is used as fuel. In the present investigation, materials are prepared according to the chemical formula $Sr_{5-x}(PO_4)_3F:Dy_x$. The mixture of reagents is mixed together to obtain a homogeneous solution. Dy_2O_3 dissolve in dil. HNO_3 solution. Fuel urea is taken in excess of the stoichiometric ratio for complete combustion. After stirring for about 30 min, the precursor solution was transferred to a furnace preheated at 500–600◦C and the porous products were obtained. The combustion reaction is roughly described as follows:

$$15Ca(NO_3)_2 \cdot 4H_2O + 9NH_4H_2PO_4 + 19NH_2CONH_2(\text{excess}) + 3NH_4F \rightarrow 3Ca_5(PO_4)_3F + 40N_2 + 19CO_2 + 71H_2O$$

3. Result and discussion

3.1. XRD analysis

This phosphor shows its characteristics of X-ray diffraction hexagonal structure with space group $P6_3/m$ and observed crystallite size of 15.3nm match with JCPDS card no. 17-0609 shown in Fig.1.

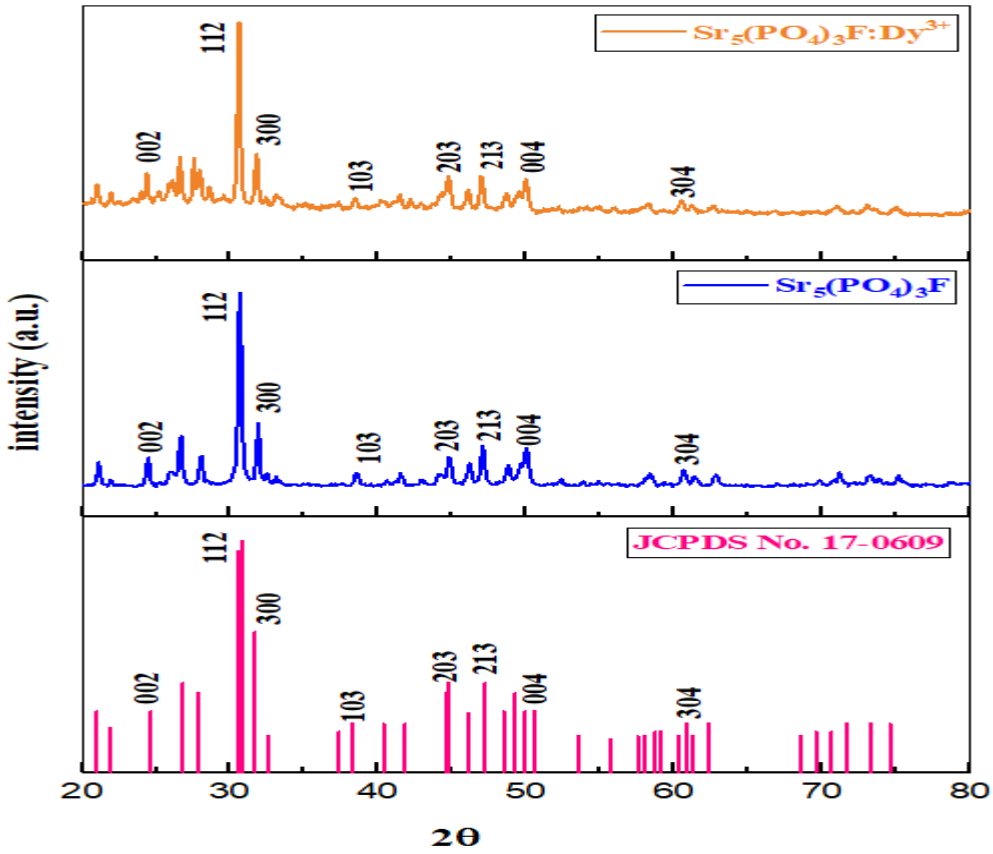

Figure: 1. XRD graph of $Sr_5(PO_4)_3F$: Dy^{3+} phosphor.

The crystal structure and structural purity of the synthesized host matrix and $Sr_5(PO_4)_3F$: Dy^{3+} phosphor were evaluated via X-ray diffraction. Fig. 1 shows a direct comparison with JCPDS Card No. 17-0609 confirms that both the pure and doped samples perfectly match the standard profiles, stabilizing in a highly crystalline hexagonal apatite framework.[13,14]. The presence of sharp, well-defined diffraction peaks corresponding to lattice planes such as (002), (112), and (300) reflects excellent crystallinity.

Table. 1 shown the hkl values and crystallite size of $Sr_5(PO_4)_3F$: Dy^{3+} phosphor, that presented quantitative analysis using the Scherrer equation across multiple lattice planes details the nanoscale dimensions of the synthesized materials. The calculated values show that the average crystallite size undergoes a minor decrease from 15.9 nm for the pure$Sr_5(PO_4)_3F$ host matrix to 15.3 nm for the $Sr_5(PO_4)_3F$: Dy^{3+} doped phosphor. This slight contraction in grain size is attributed to the localized lattice strain and stress induced when host Sr^{2+} ions are substituted by the smaller rare-earth Dy^{3+}activators, which subtly restricts crystal growth during synthesis. Crucially, the data confirms that both samples consistently maintain a highly uniform structure well within the nanoscale regime (under 20 nm).[5,15].

Table: 1. average crystallite size of $Sr_5(PO_4)_3F$: Dy^{3+} phosphor.

Name of sample	hkl	2θ	FWHM	$D = \frac{K\lambda}{\beta Cos\theta}$ Crystallite size (nm)	Avg. D (nm)
$Sr_5(PO_4)_3F$	002 112 103 302 203 300 213 004 304	24.493 30.670 38.571 40.646 43.003 31.680 47.253 50.583 60.694	0.6000 0.5000 0.6000 0.5000 0.6000 0.5000 0.6000 0.4000 0.6000	13.54880 16.47516 14.02765 16.94331 14.23083 16.51572 14.45187 21.96628 15.34272	15.9nm
$Sr_5(PO_4)_3F:Dy^{3+}$	002 112 103 302 203 300 213 004 304	24.493 30.670 38.571 40.646 43.003 31.680 47.253 50.583 60.694	0.5187 0.5586 0.5985 0.3990 0.7581 0.5187 0.5586 0.5985 0.5586	15.67241 14.74683 14.06281 21.23221 11.26303 15.92030 15.52296 14.68089 16.47983	15.3nm

3.2. FTIR analysis

The FTIR spectrum (absorbance) of the synthesized $Sr_5(PO_4)_3F$: Dy^{3+} phosphor shown in Fig.2 that exhibits a well-resolved triplet at 435, 441, and 457 cm^{-1} shown in fig.2. These peaks are successfully assigned to the bending movements of the phosphate tetrahedral (PO_4^{3-}) groups. The observed crystal splitting into three separate peaks happens because the crystal shape is slightly changed or distorted. Furthermore, the sharpness of these bands strongly verifies the formation of a highly crystalline host lattice.

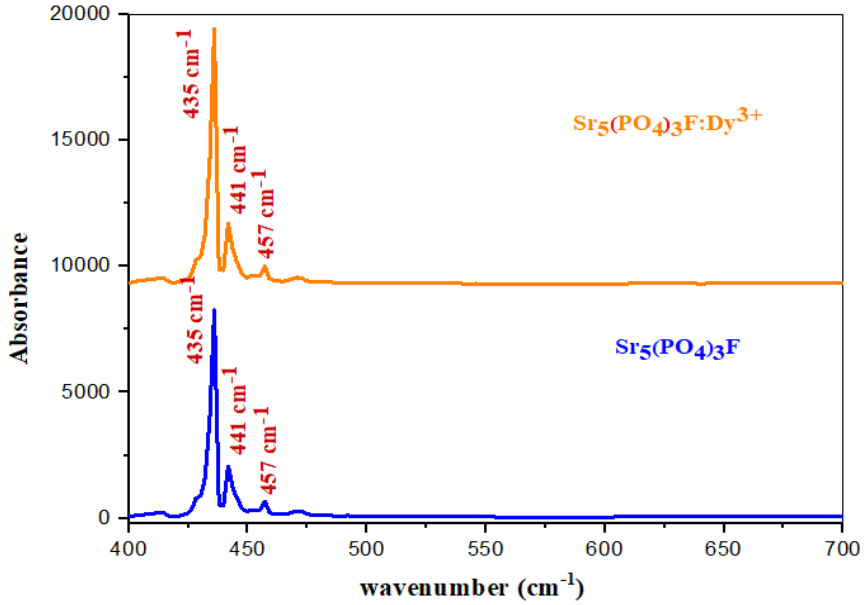

Figure: 2. Absorbance spectra of $Sr_5(PO_4)_3F$: Dy^{3+} phosphor.

3.3. SEM study

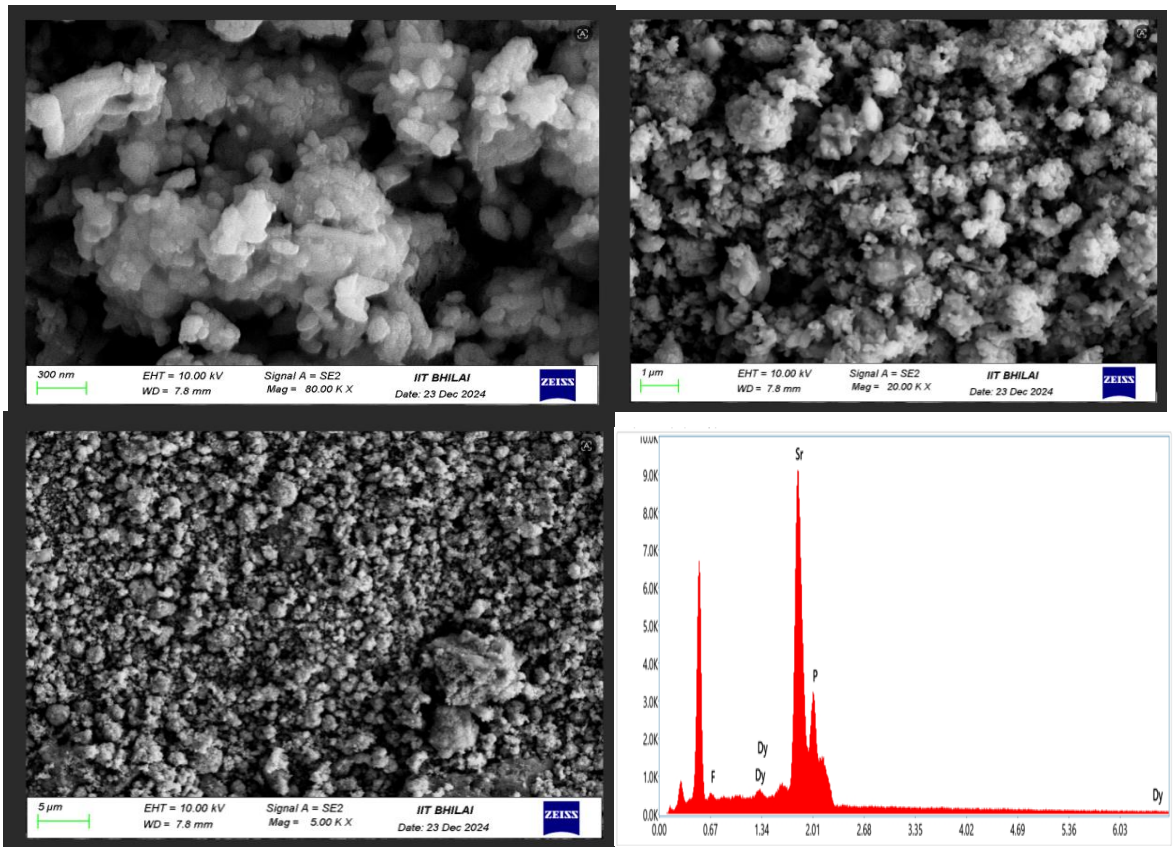

Figure: 3. SEM images of $Sr_5(PO_4)_3F$: Dy^{3+} phosphor .

SEM image was carried out to analyze the morphological study of $Sr_5(PO_4)_3F$: Dy^{3+} phosphor. Fig. 3 shows the SEM micrograph of 2 mol% Dy^{3+} doped $Sr_5(PO_4)_3F$ phosphor. The morphological analysis across multiple scales (5 µm down to 300 nm) reveals a granular, nanostructured topology. While the powder shows a tendency to aggregate into larger clusters due to high surface energy, high-magnification views confirm that individual primary particles lie well within the sub-micron and nanometer regime with heavily interconnected grain boundaries.[11,12].

Table: 2. SEM values of element of $Sr_5(PO_4)_3F$: Dy^{3+} phosphor

Element	Weight %	MDL	Atomic %	Net Int.	Error %	R	A	F
F K	0.9	0.59	3.3	23.9	9.3	0.4663	0.6867	1.0000
P K	17.8	1.38	37.9	298.1	4.2	0.5017	0.8579	1.0050
Sr L	73.9	2.38	55.8	721.2	3.1	0.4968	0.9434	1.0032
Dy L	7.4	96.57	3.0	3.3	60.8	0.9128	0.9961	1.0222

Complementing the microstructural data, the EDX profile confirms good phase purity. Strong characteristic peaks validate a host matrix composed of Strontium (Sr), Phosphorus (P), and Fluorine (F). Furthermore, the clear detection of low-intensity Dysprosium (Dy) peaks proves successful rare-earth activation within the host lattice.

3.4. PL study

3.4.1. Photo-luminescence (PL) Characteristics and Concentration Optimization

The photoluminescence (PL) properties of the synthesized phosphor doped with varying concentrations of activator ions (1 mol%, 2 mol%, 2.5 mol%, and 3 mol%) were investigated at room temperature. Fig.

5 illustrates the comprehensive PL spectrum, consisting of the photoluminescence excitation spectrum on the left and the photoluminescence emission spectrum on the right. The excitation spectrum, monitored under the dominant emission wavelength, exhibits two prominent electronic transitions centered in the near-ultraviolet (near-UV) region at approximately 350 nm and 365 nm. The presence of these sharp excitation bands indicates that the host lattice efficiently absorbs energy in the near-UV range, making this material highly compatible with commercial near-UV LED chips.

Upon exciting the phosphor at its optimal absorption threshold, the emission spectrum reveals a highly symmetric and intense emission peak localized at 575 nm. This sharp emission band falls squarely within the orange-yellow visible spectral region. The narrow full-width at half-maximum (FWHM) of the 575 nm peak reflects a well-defined local coordination environment around the doped activator ions within the host matrix, minimizing non-radiative lattice vibrations.

To identify the optimum luminescent performance, the doping concentration of the activator was systematically varied. As depicted in the spectral overlay, the PL intensity of both the excitation and emission bands escalates progressively as the dopant content increases from 1 mol% up to 2 mol%, reaching its absolute maximum at a concentration of 2 mol%. This initial increase is attributed to the increasing number of luminescent activator centers available for radiative recombination within the host structure.

However, when the concentration is pushed further to 3 mol%, a dramatic collapse in luminescent intensity is observed in both spectra. This phenomenon is a classic manifestation of concentration quenching. As the activator concentration exceeds the critical threshold of 2 mol%, the average distance between neighboring dopant ions decreases significantly. This spatial proximity triggers non-radiative energy transfer processes, such as multipolar interactions or cross-relaxation pathways, where the excitation energy is shared among adjacent ions and ultimately lost to the lattice as heat rather than being emitted as light. Consequently, 2 mol% is established as the optimal doping concentration for achieving maximum quantum efficiency in this phosphor system.

3.4.2. Excitation Mechanisms and Electronic Transitions

The room-temperature photoluminescence properties of the synthesized $Sr_5(PO_4)_3F$ host lattice doped with varying concentrations of trivalent dysprosium Dy^{3+} ions (1 mol%, 2 mol%, 2.5 mol%, and 3 mol%) were systematically recorded. As illustrated in Fig. 4, the spectral profile is divided into two distinct zones: the PL excitation spectrum on the left and the PL emission spectrum on the right.

The excitation spectrum, recorded by monitoring the characteristic yellow emission of Dy^{3+} at 575 nm, displays sharp, well-defined electronic transitions within the near-ultraviolet (near-UV) region. The two most dominant absorption peaks are centered at approximately 350nm and 365 nm. These peaks arise from the ground-state intra-configurational 4f transitions of the Dy^{3+} ions. Specifically, the sharp peak at 350nm corresponds to the $^6H_{15/2} \rightarrow {}^6P_{7/2}$ transition, while the adjacent band at 365 nm is assigned to the $^6H_{15/2} \rightarrow {}^6P_{5/2}$ transition. The intense nature of these near-UV excitation bands confirms that the strontium fluorapatite matrix provides an excellent environment for capturing light from standard commercial near-UV - LED chips, signaling its utility in solid-state lighting applications.

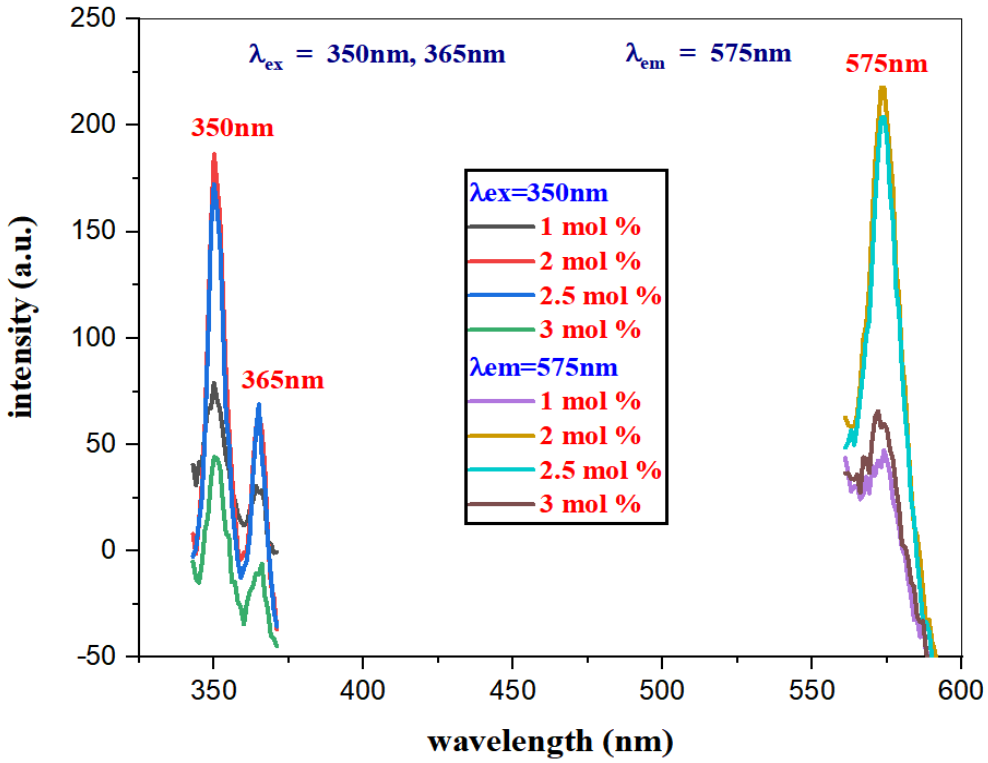

Figure: 4. PL emission and excitation spectra of $Sr_5(PO_4)_3F$: Dy^{3+} phosphor.

3.4.3. Emission Spectrum and Crystal Field Interaction

Under a steady excitation wavelength of 350nm, the emission spectrum exhibits a highly intense and symmetric peak localized in the yellow-orange visible spectrum at 575 nm. This specific emission line corresponds to the typical $^4F_{9/2} \rightarrow {}^6H_{13/2}$ transition of the Dy^{3+} activator. In lanthanide luminescence, the $^4F_{9/2} \rightarrow {}^6H_{13/2}$ transition is highly hypersensitive to the local coordination chemistry, meaning its transition probability obeys forced electric-dipole rules and relies heavily on the local asymmetry of the host site. In the hexagonal apatite framework of $Sr_5(PO_4)_3F$, the Dy^{3+} ions substitute into the low-symmetry divalent strontium Sr^{2+} sites. The high intensity and sharp full-width at half-maximum (FWHM) of the 575nm peak confirm that the dysprosium ions successfully occupy a heavily asymmetric local environment, suppressing non-radiative multi-phonon relaxation pathways.

3.4.4. Dopant Optimization and Concentration Quenching

To determine the optimum luminescent output of the system, the Dy^{3+} doping concentration was varied from 1 mol% up to 3 mol%. The spectral overlay clearly demonstrates that the emission intensity at 575nm rises continuously when moving from 1 mol% to 2 mol%, culminating in its peak efficiency at 2 mol%. This positive trend is driven by a steady expansion in the population of active luminescent centers inside the fluorophosphate matrix, resulting in more photons being radiated upon near-UV exposure.

However, a further increase in the activator concentration to 3 mol% triggers a drastic drop in the luminescence intensity across both the excitation and emission bands. This performance drop is caused by the concentration quenching effect. When the doping density surpasses the critical threshold of 2 mol%, the average spatial distance between neighboring Dy^{3+} ions shrinks significantly below the

critical transfer distance. This close proximity creates highly efficient non-radiative paths, allowing cross-relaxation or resonance energy transfer to happen between adjacent dysprosium centers. Instead of emitting yellow light via the $^4F_{9/2} \rightarrow {}^6H_{13/2}$ pathway, the stored excitation energy migrates through the dopant cluster until it hits a quenching defect site where it dissipates as non-radiative lattice heat. Consequently, 2 mol% is established as the absolute optimum concentration for maximizing the quantum efficiency of the $Sr_5(PO_4)_3F:Dy^{3+}$ phosphor.

3.4.5. CIE

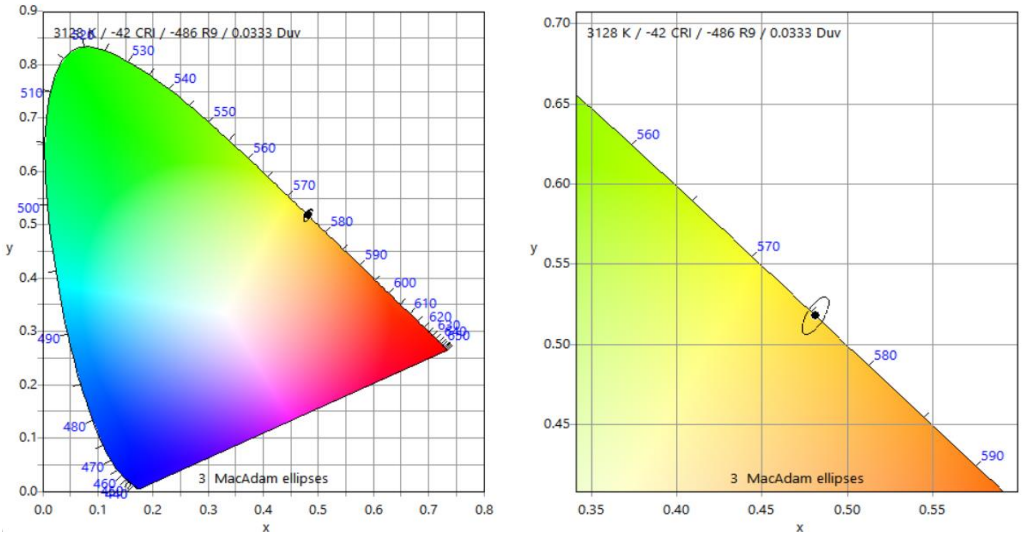

Figure: 5. CIE graph of Sr5(PO4)3F:Dy3+ phosphor

To evaluate the precise emission color quality and commercial viability of the synthesized Sr5(PO4)3F:Dy3+ phosphor for solid-state lighting, the Commission Internationale de l'Éclairage (CIE) 1931 chromaticity coordinates were calculated. The calculation was executed by integrating the relative spectral power distribution of the photoluminescence emission spectrum recorded under the optimal 350 nm near-UV excitation.

As illustrated in Fig. 5., the calculated chromaticity coordinates are located at x = 0.478 and y = 0.518. These parameters place the emission point squarely within the intense yellow region of the CIE color space diagram. The monochromatic nature of the dominant 575 nm emission, which originates from the characteristic hypersensitive $^4F_{9/2} \rightarrow {}^6H_{13/2}$ electric-dipole transition of Dy3+ ions, grants the phosphor an exceptionally high color purity.[16].

Because the emission spectrum is heavily dominated by this yellow component, the resulting light exhibits a warm chromatic profile. This localized coordinates make the $Sr5(PO4)3F:Dy^{3+}$ phosphor a highly promising candidate for developing warm-white light-emitting diodes (w-LEDs) when blended with a suitable blue-emitting component, or for direct utilization in specialized amber-yellow warning signaling systems.

Conclusion

Pure, nanostructured $Sr_5(PO_4)_3F:Dy^{3+}$ phosphors with hexagonal apatite structures were successfully synthesized, exhibiting optimal yellow-orange emission at 575 nm under near-UV excitation. The material shows potential for w-LED applications, with structural purity confirmed by XRD and

optimized luminescence at 2 mol% dopant concentration. Ultimately, the structural integrity, nanoscale grain dimensions, and high near-UV excitation compatibility demonstrate that the Sr5(PO4)3F:Dy^{3+} phosphor system is a highly viable and promising candidate for next-generation solid-state white lighting (w-LEDs) and modern display packaging.

References

1. Ju, G., et al. (2021). Progress in near-UV-excited phosphors for white light-emitting diodes. *Journal of Luminescence*, 230, 117712.
2. George, N. C., et al. (2013). Lanthanide-activated phosphors for solid-state lighting. *Annual Review of Materials Research*, 43, 481-501.
3. Xie, R. J., & Hintzen, H. T. (2013). Optical properties of next-generation solid-state lighting phosphors. *Journal of the American Ceramic Society*, 96(3), 665-687.
4. Lakshminarayana, G., et al. (2018). Structural and optical investigations of rare-earth-doped fluorophosphate matrices. *Journal of Non-Crystalline Solids*, 481, 234-245.
5. Zhang, X., et al. (2015). Synthesis and luminescence properties of hexagonal apatite fluorophosphate phosphors. *RSC Advances*, 5(22), 16789-16796.
6. Kottaisamy, M., et al. (2010). Color tuning in strontium fluorophosphate phosphors via rare-earth co-doping. *Materials Research Bulletin*, 45(8), 940-945.
7. Shrivastava, R., et al. (2019). Dysprosium-activated phosphors for solid-state lighting applications: A review. *Optics & Laser Technology*, 111, 495-512.
8. Blasse, G., & Grabmaier, B. C. (1994). *Luminescent Materials*. Springer-Verlag.
9. Huang, X., et al. (2017). Single-component white-light-emitting $Sr_5(PO_4)_3F:Dy^{3+}$ phosphors for w-LEDs. *Journal of Materials Science: Materials in Electronics*, 28(14), 10234-10241.
10. Vijayakumar, R., et al. (2023). Photoluminescence and concentration quenching mechanisms in trivalent rare-earth doped apatites. *Spectrochimica Acta Part A*, 285, 121890.
11. Jenkins, R., & De Vries, J. L. (2012). *An Introduction to X-ray Spectrometry*. Springer Science & Business Media.
12. Shrivastava, R., & Dhoble, S. J. (2019). Comprehensive overview of synthesis routes and characterization techniques for rare-earth-activated phosphors. *Optics & Laser Technology*, 111, 495-512.
13. Cullity, B. D., & Stock, S. R. (2014). *Elements of X-ray Diffraction* (3rd ed.). Pearson Education.
14. Scherrer, P. (1918). Bestimmung der Grösse und inneren Struktur von Kolloidteilchen mittels Röntgenstrahlen. *Nachrichten von der Gesellschaft der Wissenschaften zu Göttingen*, 26, 98-100.
15. Shannon, R. D. (1976). Revised effective ionic radii and systematic studies of interatomic distances in halides and chalcogenides. *Acta Crystallographica Section A*, 32(5), 751-767.
16. Commission Internationale de l'Éclairage (CIE). (1932). Commission Internationale de l'Éclairage Proceedings 1931. Cambridge University Press.